Journal of Photochemistry and Photobiology A: Chemistry 211 (2010) 176–184

Contents lists available at ScienceDirect

Journal of Photochemistry and Photobiology A: Chemistry

journal homepage: www.elsevier.com/locate/jphotochem

Molecular recognition of 2-alkylbenzimidazole: Photophysical and structural studies

Bimlesh Ojha, Gopal Das*

Department of Chemistry, Indian Institute of Technology Guwahati, Assam 781 039, India

ARTICLE INFO

Article history:
Received 1 August 2009
Received in revised form
30 December 2009
Accepted 29 January 2010
Available online 16 March 2010

Keywords:
Organic salt
Co-crystal
Electron-deficient compound
Electron-rich compound
Supramolecular chemistry
Fluorescence

ABSTRACT

2-Alkylbenzimidazole ($\mathbf{L_{1-3}}$) forms organic salt co-crystals with several electron-deficient aromatic as well as aliphatic polycarboxylic acids. Electron-rich benzimidazole shows dramatic quenching of fluorescence in presence of electron-deficient acidic guest molecules. Higher selectivity was found towards pyromellitic acid. Substituted benzimidazole forms organic salt co-crystals with different acids of general composition [$\mathbf{L_n}H^+ \cdot A^-$] (where, A is the acid molecule). The non-covalent interactions between carboxylic acids and $\mathbf{L_{1-3}}$ were investigated by UV–vis, fluorescence and ^{1}H NMR spectroscopic methods in solution and by single crystal X-ray diffraction in solid state.

1. Introduction

The development of new hosts capable to form hydrogen bonding with guest molecules in solution and their use in the construction of new chemosensors for the selective recognition of important anions is of great interest in the field of host–guest recognition chemistry. In this aspect, aromatic acids are important target anions. It is well established that the weak C–H···O hydrogen bonds extensively exist just like their strong counterparts [1,2] and are found widely in proteins and many organic crystals [3–5]. Although it is much weaker in comparison to the usual strong hydrogen bond, X–H···Y (X, Y = N, O, F), this kind of interactions have aroused significant interest in recent times. In this aspect, reports concerning the occurrence of weak C–H···O interactions in solution are still rare [6,7]. Although the idea of such C–H···O interactions are familiar [8], more recently their existence and importance as a weak, but forceful, secondary interactions have been widely accepted [9]. In molecular recognition processes the non-covalent interactions such as hydrogen bonding, aromatic π-stacking and weak intermolecular interactions (viz. C–H···π and C–H···O) play the crucial role [9]. Intermolecular interactions involving aromatic rings are important in both biological [10] and non-biological processes [11]. Much of the works have been done in the field of directed synthesis of novel host with specific properties. Within the field of supramolecular chemistry, the non-covalent interactions between a π-electron-rich donor molecules and a π-electron-deficient acceptor moiety through hydrogen bond and/or cooperative aromatic π–π interactions have attracted much attention in recent years [12].

Strong classical hydrogen bonds, such as O–H···N and O–H···O, are ideal to rationalize and systemize the relationship between hydrogen bond acceptor and donor molecules. Because of the predictable supramolecular properties and the ability to form strong and directional hydrogen bonds, dicarboxylic acids were frequently chosen as building blocks for crystal engineering [13–15], and numerous heterodimers composed of carboxylic acids and a variety of basic building blocks such as amines, dipyridines, pyrazines, and their analogues have been documented recently [16–19]. The hydrogen bonding between hydroxyl of carboxylic acids and heterocyclic nitrogen atoms has been proved to be a useful and powerful organizing force and utilized for the formation of variety of supramolecular 3D architectures. Depending on the difference in the pK_a value of the acidic and basic organic unit, they may form organic salt or co-crystal in solution or in solid state [20,21]. Benzimidazole and its derivatives are ubiquitous in biology. Their structures and functions are important in various biochemical processes. They are also important class of molecules in the field of drugs and pharmaceuticals [22–26] and have attracted special attention in the construction of some interesting 3D framework in recent years [22–26]. It is also conceivable that great efforts have been directed towards the development of organic molecular crystals containing a variety of benzimidazole architectures

* Corresponding author. Tel.: +91 361 258 2313; fax: +91 361 258 2349.
E-mail address: gdas@iitg.ernet.in (G. Das).

1010-6030/$ – see front matter © 2010 Elsevier B.V. All rights reserved.
doi:10.1016/j.jphotochem.2010.01.021

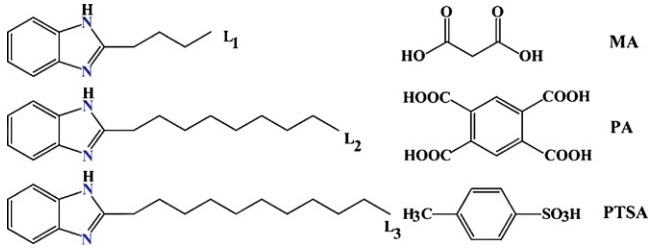

Scheme 1. Chemical Structures of $\mathbf{L_1}$, $\mathbf{L_2}$, $\mathbf{L_3}$ and acids.

[22–26]. Non-ionic surfactants belonging to 2-alkylbenzimidazole are widely used in industrial and medical applications [27]. Benzimidazole head group has several advantages viz. it can act as both hydrogen bond donor and acceptor [28–31], it has both acid and base character [32], it has intrinsic fluorescence properties [33] and it is well-known ligand for metal ions [22–26].

We are interested to explore the scope of various weak non-covalent interactions in molecular recognition processes by designing new ligands [34–38]. In this paper, we report the molecular recognition of electron-deficient aromatic acid by electron-rich 2-alkylbenzimidazole molecules ($\mathbf{L_{1-3}}$). We have determined the single crystal X-ray structure of the ligands ($\mathbf{L_{1-3}}$) and their organic salts in presence of different acidic molecules viz. oxalic acid (OA); malonic acid (MA); pyromellitic acid (PA) and *p*-toluenesulphonic acid (PTSA) to have an idea of different types of non-covalent intermolecular interactions in the solid state (Scheme 1). We have also studied the interactions of these amphiphilic molecules in solution with various other acids and their derivatives using UV-visible, steady state fluorescence and NMR spectroscopy.

2. Experimental

2.1. Materials and methods

Commercially available *o*-phenylenediamine and aliphatic acids were obtained from Sigma, USA. Other chemicals were of reagent grade and used without further purification. The absorption spectra were recorded on a *Perkin Elmer Lambda*-25 UV–vis spectrophotometer using 10 mm path length quartz cuvettes at 298 ± 0.1 K, in the range of 230–350 nm wavelengths. Fluorescence measurements were made on a *Carry eclipse* spectrofluorometer using 10 mm path length quartz cuvettes with slit width of 5 nm at 298 ± 0.1 K. NMR spectra were recorded on a *Varian* FT-400 MHz instrument. The chemical shifts were recorded in parts per million (ppm) scale using tetramethylsilane (TMS) as a reference at 298 K. Optical fluorescence micrograph images of air-dried samples on a glass micro slide were taken using a *Zeiss-Axio Cam-MRc* microscope fitted with a digital camera. Scanning electron micrograph (SEM) images of samples glued on an aluminum stub and gold sputtered were obtained by means of a *LEO-1430 VP* electron microscope. For spectral studies, the ligands and acid stock solutions were prepared in acetonitrile. In a 3 mL solution of the ligands, different concentrations of the acid were added ranging from 0.05 to 0.56 mM. After proper mixing of the solution the spectra were recorded on the spectrophotometer.

2.2. Synthesis of $\mathbf{L_1}$, $\mathbf{L_2}$ and $\mathbf{L_3}$

2-Alkylbenzimidazoles ($\mathbf{L_{1-3}}$) were prepared by the condensation of *o*-phenylenediamine and corresponding aliphatic acids according to the literature method [39,40]. The compounds were purified by re-crystallization from methanol. The compounds were also characterized by single crystal X-ray along with NMR, IR and melting point and were found to be in good agreement with the reported data (Supporting information) [39–41].

2.3. Synthesis of organic salts

Equivalent amounts of acids and ligands ($\mathbf{L_{1-3}}$) were dissolved in acetonitrile and methanol mixture at room temperature with constant stirring for a period of 3–5 h. The resulting solution was kept at room temperature for 3–7 days without any mechanical disturbance to obtain the single crystals of the corresponding salts suitable for X-ray diffraction. The organic salts isolated are: [H$\mathbf{L_1}$][Malonate] (1); [H$\mathbf{L_1}$][*p*-toluenesulphonate] (2); [H$\mathbf{L_1}$][Pyromellitate] (3); [H$\mathbf{L_2}$][Malonate] (4); [H$\mathbf{L_2}$][Pyromellitate], (5); and [H$\mathbf{L_3}$][*p*-toluenesulphonate] (6).

2.4. X-ray crystallography

The intensity data were collected using a *Bruker SMART APEX-II* CCD diffractometer, equipped with a fine focus 1.75 kW sealed tube Mo Kα radiation (λ = 0.71073 Å) at 298(2) K, with increasing ω (width of 0.3° per frame) at a scan speed of 3 s/frame. The SMART software was used for data acquisition. Data integration and reduction were undertaken with SAINT and XPREP [42] software. Multi-scan empirical absorption corrections were applied to the data using the program SADABS [43]. Crystal and molecular structures were solved by direct methods using SHELXS-97 and refined with full-matrix least squares on F^2 using SHELXL-97 [44]. All non-hydrogen atoms were refined anisotropically. The hydrogen atoms were located from the difference Fourier maps and refined isotropically. Structural illustrations have been drawn with ORTEP-3 for Windows [45].

3. Results and discussion

3.1. Supramolecular interactions in solution phase

Aromatic compounds usually have electron-deficient or electron-rich hydrophobic moieties, and therefore, aromatic molecules capable to form weak complexes via π–π stacking interactions are extremely attractive. Formation of organic salt co-crystal is an important field of research in pharmaceutical chemistry. Construction of different 3D network via variety of non-covalent interactions between organic anion and cation is a challenge to the crystal engineering. Presence of electron-rich basic benzimidazole unit in ligands ($\mathbf{L_{1-3}}$) allows us to study this phenomenon with a large variety of electron-deficient aromatic or aliphatic acids and their derivatives in solution as well as in solid state. Fig. 1a shows the UV–vis absorption spectra of the ligands in acetonitrile. The three characteristics absorptions at 243, 273 and 280 nm were observed [46,47] for the ligands in neutral medium (Fig. 1a). The UV–vis spectra of the compounds do not show any significant changes with the variation of solvent polarity as well as with alkyl chain length.

The absorption maximum of $\mathbf{L_{1-3}}$ does not show any spectral shift or appearance of a new peak when titrated with oxalic acid, malonic acid, phthalic acid and phthalic anhydride (Supporting information, Figs. S3–S5). Fig. 1b shows the UV–vis absorption spectra of ligand $\mathbf{L_1}$, with increasing concentrations of pyromellitic acid in acetonitrile. It can be seen from the figure that the absorbance of ligand increases with increasing concentrations of the acid, while the acid has one absorption at around 292 nm, showed gain in intensity upon complexation with the ligand. A reasonable explanation for the two evidences may come from the complex formation between ligand and pyromellitic acid. Similar result has been obtained with pyromellitic anhydride too (Supporting information, Fig. S3). As the acids are not soluble in non-polar solvents, we are

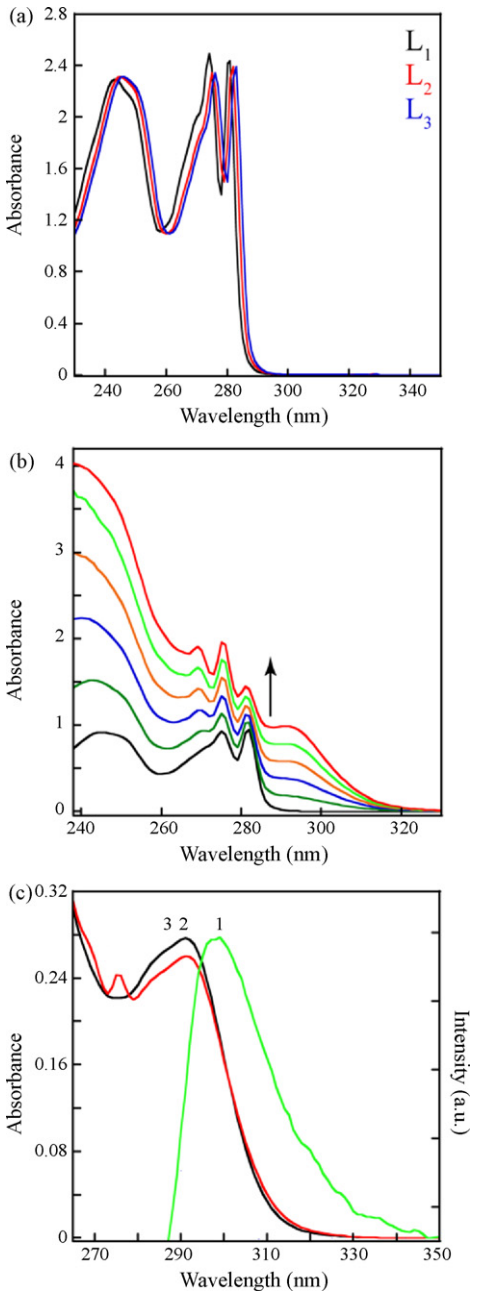

Fig. 1. (a) Absorbance spectra of $\mathbf{L_{1-3}}$ (5 mM) in acetonitrile and (b) Absorbance spectra of $\mathbf{L_1}$ (5 mM) with increasing concentrations of pyromellitic acid in the range of 0–0.25 mM and (c) emission spectra of ligand $\mathbf{L_1}$ (1), absorbance spectra of pyromellitic acid (2) and pyromellitic anhydride (3) showing the spectral overlap.

unable to do the experiment in non-polar solvents to examine the formation of a weak π-complex. Thus, these results confirmed that there are some significant ground state interactions between the ligands ($\mathbf{L_{1-3}}$) and the pyromellitic acid/anhydride.

Fig. 2a shows the emission spectra of ligands ($\mathbf{L_{1-3}}$) in acetonitrile at room temperature. The ligands shows a locally excited monomer emission at ~297 nm when excited at 270 nm, at neutral pH [46,47]. However, in presence of inorganic acid (H_2SO_4), i.e. at acidic pH, the molecules showed two emission bands at ~297 and 365 nm, respectively, when activated at 270 nm (Supporting information, Fig. S7), where the peak at 365 nm is due to the formation of benzimidazolium cation [46,47]. There is no appreciable change in the peak position due to variation of alkyl chain length, as there is a very little change in the excited state behaviour of the fluorophores and hence, the ligands have very similar chemical and physical properties [46,47]. The emission spectra of the ligands are found to be independent of solvent polarity and the intensity increases with increasing concentrations without appearance of any new peak at higher wavelengths (Supporting information, Fig. S10). The air-dried sample of $\mathbf{L_1}$ on glass surface showed blue fluorescence, when observed under optical fluorescence microscope in solid state (Fig. 2a inset). In contrast to the emission spectra in presence of inorganic acid (H_2SO_4), the changes in the fluorescence emission spectra of ligands ($\mathbf{L_{1-3}}$) in presence of organic acids are very different. When solution of ligands prepared in acetonitrile (5 mM) were titrated with different types of organic acids and their anhydrides, the fluorescence intensity was quenched to varying degrees depending on the nature of the added acid molecules without appearance of any peak at 365 nm (Fig. 2b). To investigate the selectivity and sensitivity of these electron-rich ligands towards the above mentioned acidic guest molecules, the changes in fluorescence intensity of $\mathbf{L_1}$ has been plotted as a function of concentration of the guest molecules (Fig. 2c). Upon addition of pyromellitic acid and pyromellitic anhydride to the ligands ($\mathbf{L_{1-3}}$), the intensity of emission band at ~297 nm gradually decreased without any spectral change (no spectral shifts or appearance of new emission bands) as shown in Fig. 2b. In a similar way to that described above the fluorescence intensity were not substantially change due to the addition of phthalic acid/anhydride, *p*-toluenesulphonic acid, oxalic acid and malonic acid to the ligands (Supporting information, Fig. S11). The maximum quenching of fluorescence intensity was obtained due to the addition of pyromellitic acid and pyromellitic anhydride to $\mathbf{L_{1-3}}$ (Fig. 2d). Fig. 2d clearly showed that $\mathbf{L_{1-3}}$ exhibits relatively higher selectivity towards pyromellitic acid and its anhydride over other electron-deficient aromatic as well as aliphatic acids in term of quenching percentage. Pyromellitic anhydride quenches the fluorescence emission by ~82%, whereas for pyromellitic acid the quenching was much more pronounced (~90%). The difference in quenching behaviour can be rationalized by the difference in complex forming ability of these guest molecules with the ligands ($\mathbf{L_{1-3}}$). In the absence of organic acid, intrinsic fluorescence of the ligands displayed typical emission spectrum with emission maxima around at 297 nm, while pyromellitic acid, pyromellitic anhydride and phthalic acid shows an intense absorption in the UV region at around 292 and 280 nm, respectively. As shown in Fig. 1c the absorption spectrum of pyromellitic acid and anhydride extensively overlaps with the emission spectra of the ligands. Altogether, these results indicate that the quenching of ligand fluorescence was due to a non-radiative energy transfer between pyromellitic acid/anhydride and ligands. In case of ligands and pyromellitic acid/anhydride the spectral overlap is quite large compared to phthalic acid and PTSA where, the spectral overlap is very less (Supporting information, Fig. S6). Thus, resonance energy transfer is enhanced in case of pyromellitic acid/anhydride compare to other acids used. The larger overlap between emission spectra of ligands and absorbance spectra of pyromellitic acid/anhydride compared to other acids indicate that pyromellitic acid/anhydride should show more fluorescence-quenching effect. This indeed was the observation as shown in Fig. 2, where fluorescence of the ligand was quenched more in presence of pyromellitic acid/anhydride than in presence of other acids (Supporting information, Fig. S12). Electron-deficient pyromellitic acid can form non-covalent interactions like hydrogen bonding with electron-rich basic ligands ($\mathbf{L_{1-3}}$) and also have aromatic π–π stacking interactions (Fig. 3), whereas electron-deficient pyromellitic anhydride can have only the latter interactions. Thus, it can be concluded that quenching is the cumulative effect of both acid–base and aromatic π–π stacking interactions as shown in Fig. 3.

On the basis of the relationship between quenching of excited states of benzimidazole and the quencher concentration, the

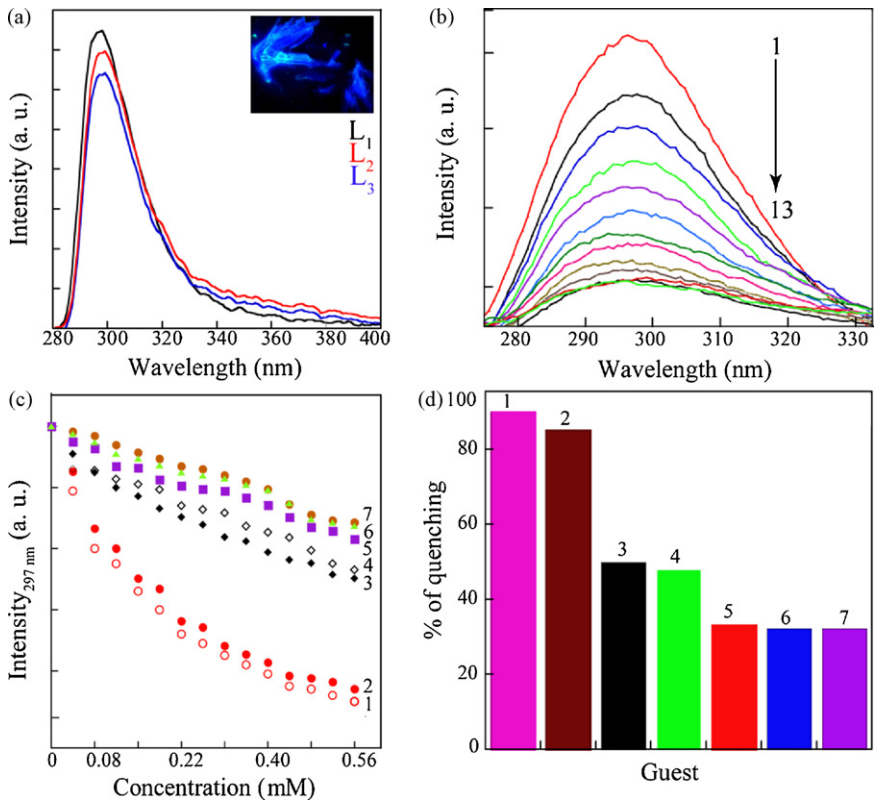

Fig. 2. (a) Emission spectra of $\mathbf{L_{1-3}}$ in acetonitrile (inset: fluorescence microscope image of $\mathbf{L_1}$); (b) emission spectra of $\mathbf{L_1}$ with increasing concentrations of pyromellitic acid and (c) changes in the fluorescence emission intensity at 297 nm of $\mathbf{L_1}$ upon addition of different acids and (d) Stack plot showing the extent of quenching by different acid molecules; where pyromellitic acid (1), pyromellitic anhydride (2), phthalic acid (3), phthalic anhydride (4), malonic acid (5), *p*-toluene sulphonic acid (6) and oxalic acid (7); [$\mathbf{L_1}$]: 5 mM and [acid]: 0–0.56 mM.

Stern–Volmer equation is given by [48]

$$\frac{F_0}{F} = 1 + K_{SV}[Q] \quad (1)$$

where F_0 and F are the relative fluorescence intensity in absence and presence of quencher, respectively and [Q] is the concentration of the quencher. K_{SV} is the Stern–Volmer quenching constant which measures the efficiency of quenching. Fig. 4a shows the Stern–Volmer plots of F_0/F versus concentration of quencher. The figure clearly shows that the degree of fluorescence quenching varied with the type of acid molecules used. It also shows that the Stern–Volmer plots are linear for oxalic acid, malonic acid, phthalic acid/anhydride and PTSA. With increasing concentrations of the guest molecules the plots do not deviate from linearity, while those of pyromellitic acid and its anhydride deviate from linearity, revealing that their interactions with $\mathbf{L_{1-3}}$ are stronger compared to the other acids used. In Table 1, the binding constants obtained from the Stern–Volmer method are listed for different guest molecules. The highest value of K_{SV} was found for the pyromellitic acid, which also showed the maximum quenching of fluorescence intensity. For the static quenching process, under the assumption that benzimidazole head group has the same and independent binding sites, the following equation was employed for the determination of binding constant or association constant (K_A) and binding sites (n) [49,50]:

$$\log\left[\frac{F - F_{\min}}{F_{\max} - F}\right] = n \log[Q] - \log K_A \quad (2)$$

Fig. 4b shows the plot of $\log[(F - F_{\min})/(F_{\max} - F)]$ versus $\log[Q]$. To determine K_A and n via a Hill plot, the expression on the left hand side of Eq. (2) is plotted as a function of log of quencher concentration. From the slope of this linear graph, a value for n can be derived, while the intersection with the abscissa corresponds to $(\log K_A)/n$. The obtained binding constants K_A and number of binding sites n were shown in Table 1. The association constants calculated for the ligand-acid/anhydride suggest low binding affinity. However lower binding constants (10^4–10^5 M^{-1}) were recently reported for several other complexes using the fluorescence spectroscopic method which correlates with our results [51–54]. Thus, it was found that the binding constant for pyromellitic acid is larger than other acid/anhydride molecules used. The number of binding sites obtained for pyromellitic acid and pyromellitic anhydride is more than one, while for other acids it is close to one. The binding

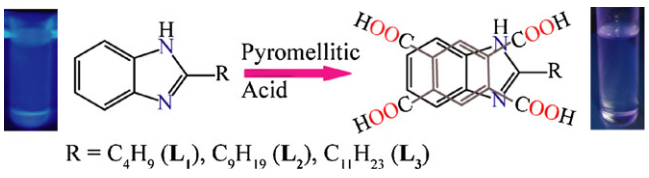

Fig. 3. Schematic illustration showing the fluorescence quenching of the ligands by pyromellitic acid due to aromatic interactions.

Table 1
Stern–Volmer (K_{SV}) and binding constant (K_A) of $\mathbf{L_1}$ with the different acid/derivatives molecules.

Sample	K_{SV} (M^{-1})	K_A (M^{-1})	n
$\mathbf{L_1}$ + pyromellitic acid	5.64×10^3	3.05×10^3	1.7
$\mathbf{L_1}$ + pyromellitic anhydride	3.50×10^3	2.50×10^3	1.6
$\mathbf{L_1}$ + phthalic acid	1.67×10^3	0.07×10^3	1.3
$\mathbf{L_1}$ + phthalic anhydride	1.32×10^3	0.05×10^3	1.2
$\mathbf{L_1}$ + PTSA	0.82×10^3	0.04×10^3	1.3
$\mathbf{L_1}$ + malonic acid	0.75×10^3	0.01×10^3	1.5
$\mathbf{L_1}$ + oxalic acid	0.53×10^3	0.02×10^3	1.4

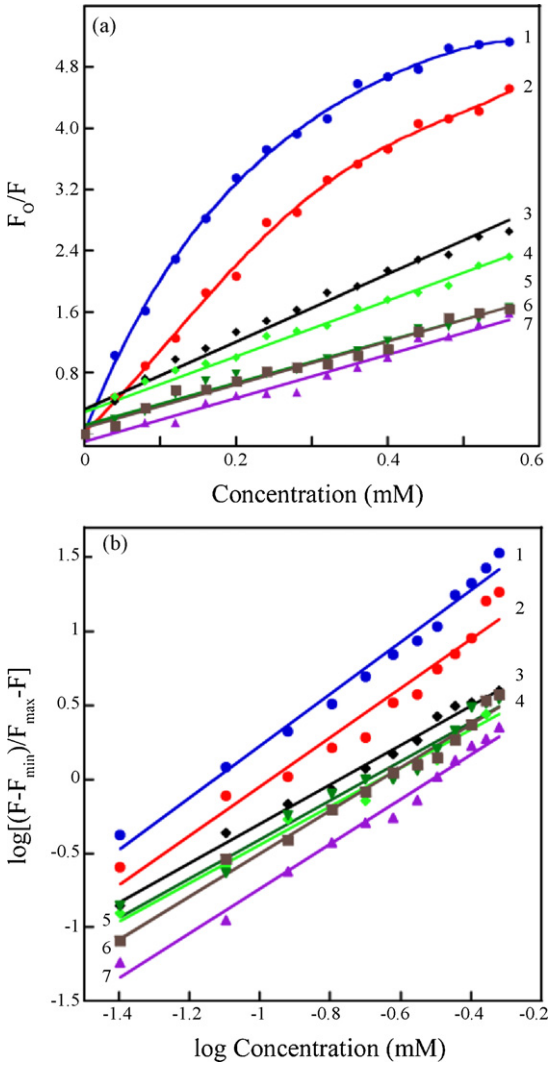

Fig. 4. (a) Stern–Volmer plot for the ligands-guest acid/derivatives complex and (b) plot of $\log[(F-F_{min})/(F_{max}-F)]$ vs. log the concentration of acid/anhydride, where pyromellitic acid (1), pyromellitic anhydride (2), phthalic acid (3), phthalic anhydride (4), malonic acid (5), PTSA (6) and oxalic acid (7).

constant values of these acids and their derivatives with $\mathbf{L_2}$ and $\mathbf{L_3}$ were also evaluated by fluorescence titration methods considering the change in emission at ~297 nm and showed similar trends to those obtained for $\mathbf{L_1}$.

To investigate the binding interactions and stoichiometries of the adduct formation in solution, we recorded ^{1}H NMR of $\mathbf{L_1}$ and its 1:1 adduct with pyromellitic acid in CD_3OD (Fig. 5). In solution the carboxyl protons of pyromellitic acid have transferred to the benzimidazole unit of the ligand molecule, resulting in the formation of benzimidazolium-pyromellitate salts in which the hydrogen-bonding donors and acceptors reside separately on the cations and anions. The chemical shifts of four H atoms of benzimidazole ring showed downfield shifts because of the cation formation. Especially, the Bz-NH, Bz-5H, Bz-6H and methylene-CH have shifts from 4.95 to 5.00, 7.47 to 7.52, 7.16 to 7.25 and 2.87 to 2.94 ppm, respectively. Surprisingly, the other methylene protons do not show any change in its chemical shift values thereby indicating its non-involvement in adduct formation in solution.

The morphologies of the crystalline materials were recorded using scanning electron microscope, and SEM images of the samples are given in Fig. 6. $\mathbf{L_1}$ alone shows the formation of micron sized rectangular stacked plates (Fig. 6a) and at 1:1 ratio with pyromellitic acid, the morphology remains same as that of $\mathbf{L_1}$ (Fig. 6b). However, at 1:5 ratios the morphology is governed by the guest molecule and it changes to sharp needles of average thickness 25 μm (Fig. 6c). At very high concentration of acid, only bulk precipitates (Fig. 6d) appears, no crystalline nature was observed. It is very clearly evident from the SEM images that the molecule has a very effective structure directing agent and the $\mathbf{L_1}$/acid ratio plays a major role in the formation of various types of microcrystalline structures.

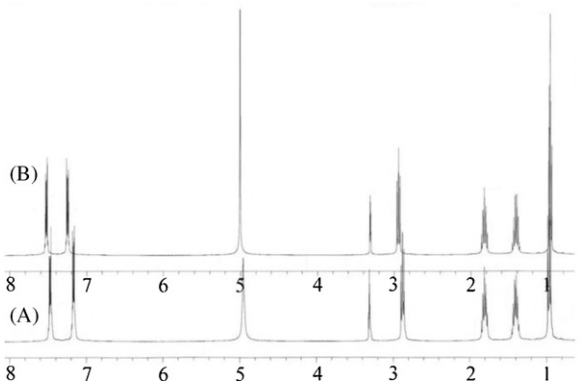

Fig. 5. ^{1}H NMR spectra (400 MHz, CD_3OD, 298 K) of $\mathbf{L_1}$ (A) and Salt 3 (B).

3.2. Supramolecular interactions in solid state

Some of our main concerns have been to ascertain the 3D organization of the organic cation and anion of an organic salt in the solid state and the consequences of weak intermolecular forces between them on the 3D network structures. Single crystal structural analysis [55] confirmed the 3D supramolecular self-organization of the organic salts formed between basic ligands ($\mathbf{L_{1-3}}$) and different aliphatic and aromatic polycarboxylic acids. ORTEP plots of these amphiphilic ligands ($\mathbf{L_{1-3}}$) are shown in Fig. 7a. We anticipated that the crystals was formed by slow evaporation of solvent, constructed by strong charge assisted N–H···O rather than less energetically favorable N···H–O interactions in neutral complexes. The schematic representations of the hydrogen bond synthons and non-bonded interactions in these ligands and their salts are listed in Supporting information (Tables S1 and S2).

Benzimidazole unit can act both as a hydrogen bond donor and acceptor. In all three ligands the benzimidazole head group is intermolecularly hydrogen bonded with the neighboring benzimidazole unit via strong N–H···N hydrogen bond. The strength of the hydrogen bond is almost comparable in all three cases. They form an infinite hydrogen bonded 1D-chain along *b* axis and the aromatic rings in the superstructures are arranged in an alternate fashion along the 1D-chain (Fig. 7b). $\mathbf{L_1}$ and $\mathbf{L_3}$ also form weak intermolecular C–H···π non-covalent interactions in solid state, where as similar type of interaction is absent in $\mathbf{L_2}$. Planar head group in each of these molecules form a V-shaped pattern, which propagates in a zigzag fashion (Supporting information, Fig. S20). However, with increasing hydrophobic chain length, the thickness of the hydrophobic layer has increased considerably, which in turn separate the V-shaped hydrophilic layer to a greater extent. $\mathbf{L_2}$ and $\mathbf{L_3}$ packed in the crystal lattice with distinct alternating hydrophobic and hydrophilic layer because of comparatively longer chain length compared to $\mathbf{L_1}$ (Fig. 7c), where the hydrophobic layer is not so prominent (Supporting information, Fig. S21).

Crystallization of $\mathbf{L_{1-3}}$ in presence of various organic acids results in the formation of organic salts. Structural analysis of these salts reveals that benzimidazole head group is mono protonated to form cation while carboxylic acid is de-protonated to form anion,

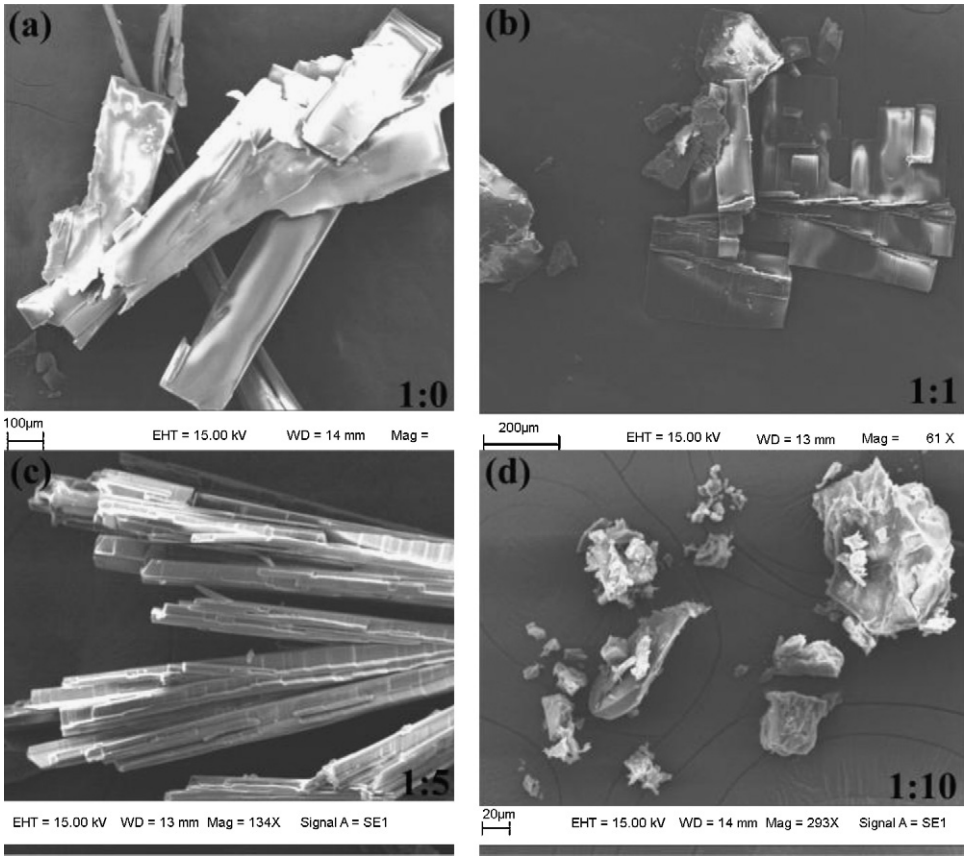

Fig. 6. (a–d) SEM images of microcrystalline $\mathbf{L_1}$ with various ratio between $\mathbf{L_1}$ and pyromellitic acid.

where the hydrogen bond donors and acceptors reside separately on the cations and anions (Scheme 2), respectively. In the next section we have described the crystal structures of the six salts formed by the various combinations of basic amphiphilic ligands with different organic acids. The various types of non-bonded interactions present in the salts are listed in Supporting information (Table S2).

[H$\mathbf{L_1}$]Malonate (Salt 1) crystallizes in monoclinic *Cc* space group with mono de-protonated malonate in the crystal lattice (Fig. 8a). In solid-state benzimidazolium cations and malonate anions are self-assembled to form an infinite 1D N–H···O hydrogen bonded chain along the diagonal of *ac* plane. It also has C–H···O interactions in the solid state. Along *b* axis, H$\mathbf{L_1}^+$ forms an inter-connecting zigzag chain which leaves a hexagonal honey comb channel running through *a* axis (Supporting information, Figs. S22 and S14), filled with a pair of malonate anions, while the alkyl chain of $\mathbf{L_1}$ is clipping the pairs of anions together (Fig. 8a).

[H$\mathbf{L_1}$]*p*-Toluenesulphonate (Salt 2) crystallizes in orthorhombic *Fdd*2 space group, where the protonated benzimidazole head group forms strong N–H···O hydrogen-bonding interactions with sulphonate group (Fig. 8b). The infinite 1D hydrogen bonded chain propagates along the diagonal of *ac* plane, while the methyl group in the para position of the anion forms C–H···π interactions with π-electron clouds of the cationic benzimidazole unit. Sulphonate anion also forms C–H···O non-covalent interactions with the neighboring cationic head group of the ligand (Supporting information, Fig. S23). The hydrophobic alkyl group of cations and tolyl group of anions are packed in the same region of the crystal lattice and formed a thick hydrophobic layer, where polar part of the anions and cations are aligned in a thin layer that results in the formation of a channel like architecture along *a* axis (Fig. 8b).

[H$\mathbf{L_1}$]Pyromellitate (Salt 3) crystallizes in triclinic *P*-1 space group, where the asymmetric unit contains four H$\mathbf{L_1}^+$ cations and two doubly de-protonated pyromellitate anions (Supporting information, Fig. S16). Benzimidazole N–H proton forms strong N–H···O hydrogen bonds with the adjacent carboxylate group of the anions. However, some of the N–H protons are involved in the formation of two such types of hydrogen bonds simultaneously, which results in the formation of a 2D hydrogen bonded sheet along the diagonal of *bc* plane (Supporting information, Fig. S24). Here the anions exits in a pair of pockets surrounded by the protonated $\mathbf{L_1}$ (Fig. 9b) and the elliptical channel is running along *c* axis and the adjacent pockets are separated by protonated ligands (Fig. 9b). However, due to displacement of the aromatic rings, no π-stacking interaction is observed in the solid state.

Unlike Salt 1, [H$\mathbf{L_2}$]Malonate (Salt 4) crystallizes in symmetric triclinic *P*-1 space group, where mono de-protonated malonate anion forms strong hydrogen bond at both ends, with both N–H of the protonated ligand (Supporting information, Fig. S17). The salt forms an infinite 1D hydrogen bonded chain along *b* axis, which are interlinked among themselves via several C–H···O interactions, while the alkyl chains in the adjacent layers are oriented in an opposite direction. The protonated ligand is stacked in a head-to-head and tail-to-tail fashion and the alternate hydrophobic and hydrophilic layers are formed in the crystal lattice (Supporting information, Fig. S25).

Like Salt 3, [H$\mathbf{L_2}$]Pyromellitate (Salt 5) also crystallizes in triclinic *P*-1 space group and the asymmetric unit contains four H$\mathbf{L_2}^+$ cations and two doubly de-protonated pyromellitate anions (Supporting information, Fig. S18). The N–H protons of H$\mathbf{L_2}^+$ cations form strong N–H···O hydrogen bonds with the adjacent carboxylate anions of the acid, which results in the formation of a 2D hydrogen bonded sheet (Supporting information, Fig. S26), where the pyromellitate anions exits in a pair of hydrophilic pockets surrounded by the protonated ligands. This circular channel runs along *c* axis and the

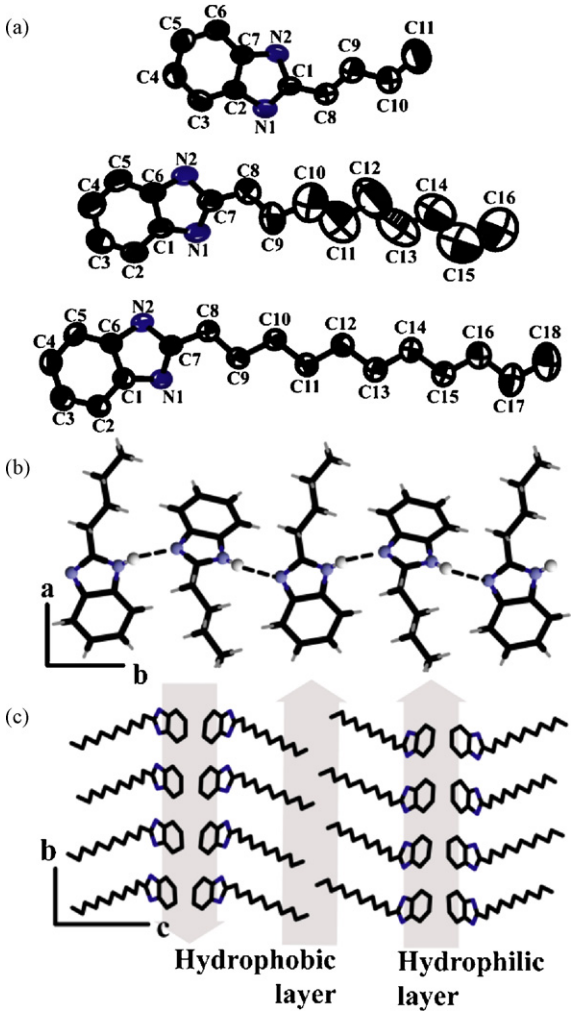

Fig. 7. (a) ORTEP plots of $\mathbf{L_{1-3}}$ with atom numbering scheme at 50% ellipsoids probability level and hydrogen atoms have been removed for simplicity; (b) 1D hydrogen bonded chain in $\mathbf{L_1}$ and (c) packing diagram $\mathbf{L_3}$ with alternating hydrophobic and hydrophilic layers.

adjacent pockets are oriented in a zigzag fashion (Fig. 9d). However, unlike Salt 3, the pyromellitate anions in Salt 5 are stacked together through aromatic π–π interactions (3.638 Å).

Unlike Salt 2, [H$\mathbf{L_3}$]*p*-Toluenesulphonate (Salt 6) crystallizes in monoclinic *C*2/*c* space group with a water molecule incorporated in the asymmetric unit (Supporting information, Fig. S19), where the protonated benzimidazole head group forms square hydrogen bonded networks through strong N–H···O interactions with sulphonate group of anions. The sulphonate anions also form strong hydrogen-bonding interactions with water molecules (Supporting information, Fig. S27). However, the methyl group in the para position of the anion does not form C–H···π interactions with π-electron clouds of the cationic benzimidazole unit unlike Salt 2, probably because of the increase in the alkyl chain length, which hindered the approach of benzimidazole unit from the back side to the anion. Similar to Salt 2, the hydrophobic part of both anions and cations are stacked in the crystal lattice and form a thick hydrophobic layer (Supporting information, Fig. S19). Hydrophilic part of the ligand aligned as a thin layer along *a* axis, which results in the formation of hydrophilic channel similar to Salt 2. But, in this case the channel is filled with water molecules. Overall the network has several N–H···O and C–H···O interactions, where the anions are oriented in the subsequent layers in a face-to-face and tail-to-tail fashion. The increased hydrophobic chain length helps to form

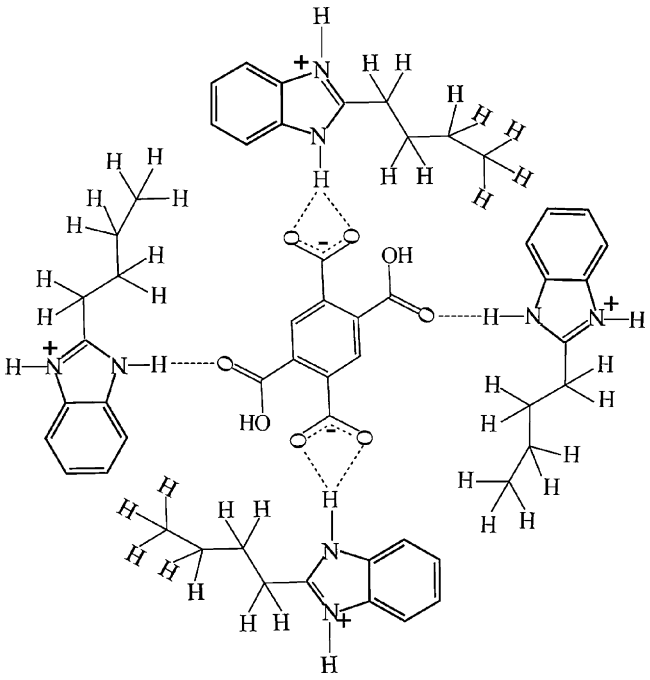

Scheme 2. Hydrogen-bond synthons of ligand ($\mathbf{L_1}$) with pyromellitic acid.

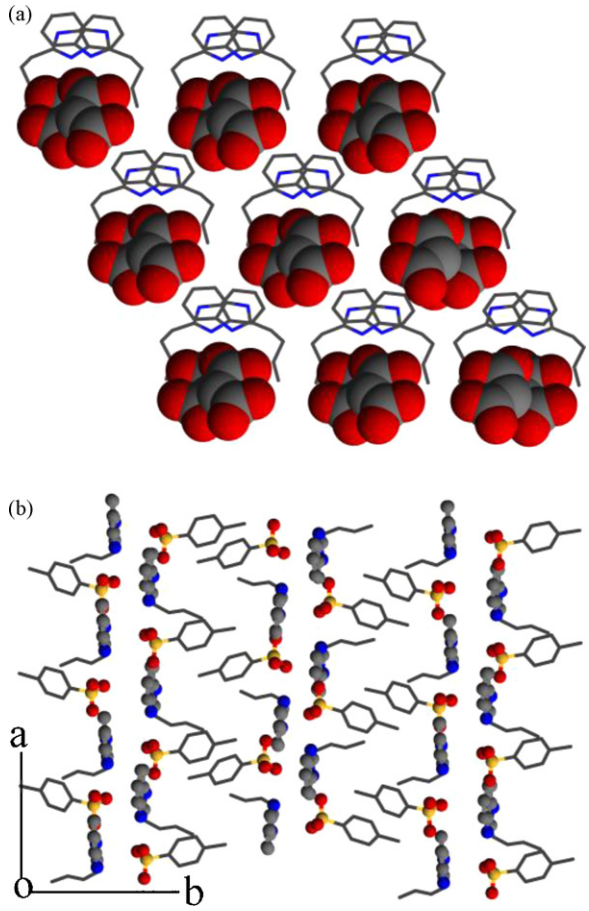

Fig. 8. Packing diagram of (a) Salt 1 along *c* axis and (b) Salt 2 along *c* axis.

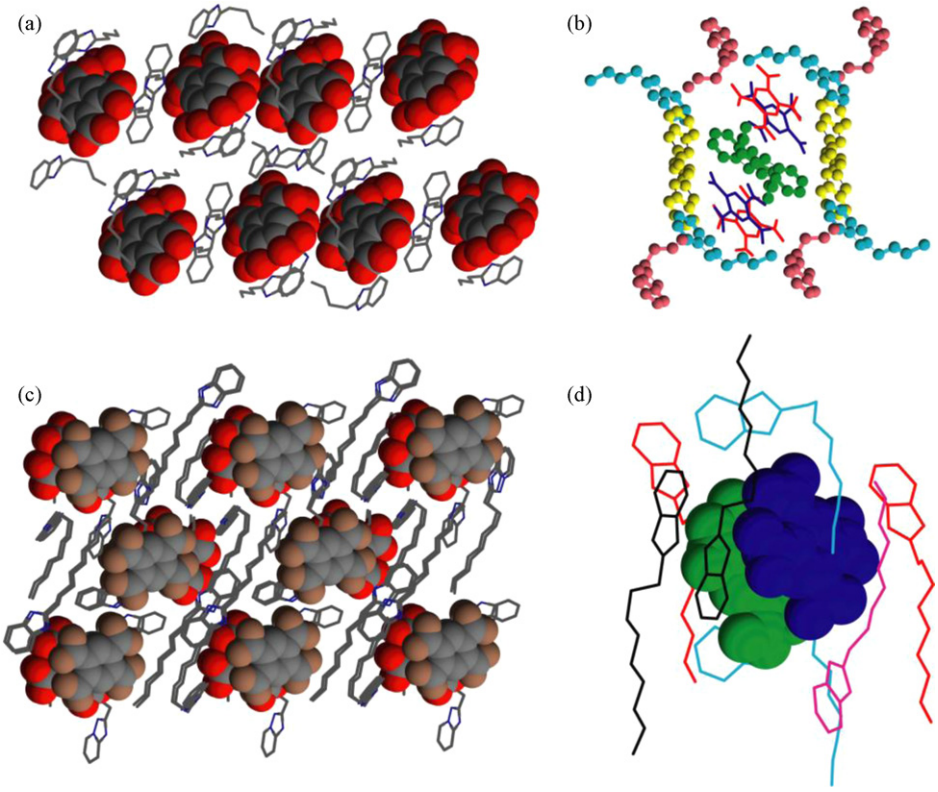

Fig. 9. (a and b) Packing diagram of Salt 3 along *c* axis; (c and d) packing diagram of Salt 5 along *a* axis.

denser and thicker hydrophobic layer in the lattice as compared to Salt 2 (Supporting information, Fig. S19).

4. Conclusions

In summary, we have synthesized 2-alkyl benzimidazole ligands of various chain lengths ($\mathbf{L_{1-3}}$) which are basic and electron-rich molecules with intrinsic fluorescence property. We have found that fluorescence properties of these ligands were highly affected by organic acids to different extent. Fluorescence-quenching efficiency of these molecules depends on the extent of electron deficiency of the guest molecules coupled with their acidic nature. Guest molecules having protected acid group with similar extent of electron deficiency can also quench the fluorescence to a similar extent. Electron-rich $\mathbf{L_{1-3}}$ can form strong intermolecular interactions with aromatic acid bearing a stronger electron-withdrawing group in solution. Thus, it has been suggested that fluorescence quenching of these molecules is a cumulative effect of both acid–base and aromatic interactions in solution. Solid-state structures of these molecules give a clue to the types of non-covalent supramolecular interactions that play role in self-assembly. We have also shown structurally, the formation of organic salts in the solid state between these basic molecules ($\mathbf{L_{1-3}}$) and the different types of acid molecules. The 3D self-assembled structures exhibit a number of weak non-covalent interactions in addition to conventional hydrogen bonding. Additionally, this study shows that benzimidazole unit is a good supramolecular building module that can produce bimolecular co-crystals, and its modular nature makes it possible to select a comfortable configuration in the course of formation of hydrogen bonds with acids. As expected, the N atom of benzimidazole ring always acts as an excellent hydrogen-bonding donor or acceptor by the formation of a strong O–H···N or ionic N–H···O hydrogen bond. In our laboratory designing of supramolecular architectures and fluorescence signaling systems for other organic molecules are currently in progress.

Acknowledgements

We thank CSIR (01-2235/08/EMR-II) and DST (SR/S1/IC-01/2008), New Delhi, India for financial support. We also thank DST-FIST for single crystal X-ray diffractometer facility. BO thanks IIT Guwahati for the fellowship.

Appendix A. Supplementary data

Supplementary data associated with this article can be found, in the online version, at doi:10.1016/j.jphotochem.2010.01.021.

References

[1] G.R. Desiraju, Acc. Chem. Res. 35 (2002) 565–573.
[2] P. Hobza, Z. Havlas, Chem. Rev. 100 (2000) 4253–4264.
[3] T. Steiner, W. Saenger, J. Chem. Soc., Chem. Commun. 20 (1995) 2087–2088.
[4] P.K. Thallapally, A.K. Katz, H.L. Carrell, G.R. Desiraju, Cryst. Eng. Commun. 5 (2003) 87–92.
[5] C. Schmuck, J. Lex, Eur. J. Org. Chem. 8 (2001) 1519–1523.
[6] M.T. Huggins, D.A. Lightner, J. Org. Chem. 66 (2001) 8402–8410.
[7] M.P.M. Marques, A.M.A. da Costa, P.J.A. Ribeiro-Claro, J. Phys. Chem. A 105 (2001) 5292–5297.
[8] D.J. Sutor, Nature 195 (1962) 68–69.
[9] G.R. Desiraju, T. Steiner, The Weak Hydrogen Bonds in Structural Chemistry and Biology, Oxford University Press, Oxford, 1999.
[10] E.A. Meyer, R.A. Castellano, F. Diederich, Angew. Chem. Int. Ed. Engl. 42 (2003) 4120.
[11] L.J. Prins, D.N. Reinhoudt, P. Timmerman, Angew. Chem. Int. Ed. Engl. 40 (2001) 2382–2426.
[12] C.K. Frederik, J. Mikkel, J. Org. Chem. 66 (2001) 6169–6173.
[13] E. Weber, Design of Organic Solids: Topics in Current Chemistry, Springer, Berlin, 1998.
[14] B.R. Bhogala, Cryst. Growth Des. 3 (2003) 547–554.
[15] X.L. Zhang, X.M. Chen, Cryst. Growth Des. 5 (2005) 617–622.
[16] V.R. Pedireddi, S. Chatterjee, A. Ranganathan, C.N.R. Rao, J. Am. Chem. Soc. 119 (1997) 10867–10868.

[17] T.R. Shattock, P. Vishweshwar, Z.Q. Wang, M.J. Zaworotko, Cryst. Growth Des. 5 (2005) 2046–2049.
[18] B.R. Bhogala, S. Basavoju, A. Nangia, Cryst. Growth Des. 5 (2005) 1683–1686.
[19] M. Sarkar, K. Biradha, Cryst. Growth Des. 6 (2006) 202–208.
[20] P.M. Bhatt, N.V. Ravindra, R. l Banerjeea, G.R. Desiraju, Chem. Commun. 8 (2005) 1073–1075.
[21] G.R. Desiraju, Cryst. Eng. Commun. 5 (2003) 466–467.
[22] S.N. Lin, L. Yang, Tetrahedron Lett. 46 (2005) 4315–4319.
[23] J. Valdez, R. Cedillo, A.H. Campos, L. Yepez, F.H. Luis, G.N. Vazquez, A. Tapia, R. Cortes, M. Hernandezc, R. Castillo, Bioorg. Med. Chem. Lett. 12 (2002) 2221–2224.
[24] G. Xue, J. Zhang, G. Shi, Y. Wu, B. Shuen, J. Chem. Soc., Perkin Trans. 2 (1989) 33–36.
[25] Z. Chen, D.J. Xu, Z.Y. Li, J.Y. Wu, M.Y. Chiang, J. Coord. Chem. 56 (2003) 253–259.
[26] J.R. Su, D.J. Xu, J. Coord. Chem. 57 (2004) 223–229.
[27] M. Alamgir, D.C. Black, N. Kumar, Topics in Heterocyclic chemistry, Springer, Berlin/Heidelberg, 2007.
[28] T. Akutagawa, T. Hasegawa, T. Nakamura, G. Saito, Cryst. Eng. Commun. 5 (2003) 54–57.
[29] J.R. Ferrer, P.M. Lahti, C. George, P. Oliete, M. Julier, F. Palacio, Chem. Mater. 13 (2001) 2447–2454.
[30] P.M. Lahti, J.R. Ferrer, C. George, P. Oliete, M. Julier, F. Palacio, Polyhedron 20 (2001) 1465–1473.
[31] Z. Liu, Y. Chen, P. Liu, J. Wang, M. Huang, J. Solid State Chem. 178 (2005) 2306–2312.
[32] P. Chowdhury, S. Panja, A. Chatterjee, P. Bhattacharya, S. Chakravorti, J. Photochem. Photobiol. 170 (2005) 131–141.
[33] M. Krishnamurthy, P. Phaniraj, S.K. Dogra, J. Chem. Soc. Perkin Trans. 2 (1986) 1917–1925.
[34] A. Pramanik, G. Das, Cryst. Growth Des. 8 (2008) 3107–3113.
[35] A. Pramanik, M. Bhuyan, G. Das, J. Photochem. Photobiol. A 197 (2008) 149–155.
[36] H. Thakuria, B.M. Borah, A. Pramanik, G. Das, Tetrahedron Lett. 47 (2006) 3135–3138.
[37] A. Pramanik, M. Bhuyan, R. Choudhury, G. Das, J. Mol. Struct. 879 (2008) 88–95.
[38] H. Thakuria, B.M. Borah, A. Pramanik, G. Das, J. Chem. Crystallogr. 37 (2007) 807–816.
[39] R. Seka, R.H. Muller, Monatsh, Chem. 57 (1931) 95.
[40] W.O. Pool, J.H. Harwood, A.W. Ralston, J. Am. Chem. Soc. 59 (1937) 178–179.
[41] Z.Z. Hui, Y. Liang, W.Y. Mei, Catal. Commun. 8 (2007) 1126–1131.
[42] SMART, SAINT and XPREP, Siemens Analytical X-ray Instruments Inc., Madison, Wisconsin, USA, 1995.
[43] G.M. Sheldrick, SADABS: software for Empirical Absorption Correction, University of Gottingen, Institute fur Anorganische Chemieder Universitat, Tammanstrasse 4, D-3400 Gottingen, Germany, 1999–2003.
[44] G.M. Sheldrick, SHELXS-97, University of Gottingen, Germany, 1997.
[45] L.J. Farrugia, J. Appl. Crystallogr. 30 (1997) 565.
[46] M. Kondo, H. Kuwano, Bull. Chem. Soc. Jpn. 42 (1969) 1433–1435.
[47] K.S. Rogers, C.C. Clayton, Anal. Biochem. 48 (1972) 199–201.
[48] J.R. Lakowicz, Principles of Fluorescence spectroscopy, 2nd ed., Kluwer Academic/Plenum, New York, 1999.
[49] E. Cielen, A. Tahri, K.V. Heyen, G.J. Hoornaert, F.C. De Schryver, N. Boens, J. Chem. Soc. Perkin Trans. 2 (1998) 1573–1580.
[50] A. Prasanna de Silva, H.Q. Nimal Gunaratne, J. Chem. Soc., Chem. Commun. 2 (1990) 186–188.
[51] D.A. Jose, D.K. Kumar, B. Ganguly, A. Das, Tetrahedron Lett. 46 (2005) 5343–5346.
[52] K. Ghosh, G. Masanta, Tetrahedron Lett. 49 (2008) 2592–2597.
[53] K. Ghosh, T. Sena, R. Frohlichb, Tetrahedron Lett. 48 (2007) 7022–7026.
[54] J. Shao, Y. Qiao, H. Lin, H. Lin, J. Fluoresc. 19 (2009) 183–188.
[55] Crystal data for **L_1**: $C_{11}H_{13}N_2$, CCDC #736542; M = 173.23, orthorhombic, a = 8.5337(4), b = 9.8356(4), c = 24.4752(13) Å, V = 2054.30(17) Å^3, space group *Pbca*, Z = 8, T = 298(2) K, μ (Mo-Kα) = 0.065 mm^{-1}, F(0 0 0) = 837, GOF = 1.076; final R indices: $R1$ = 0.0481 [$I > 2\sigma(I)$], $wR2$ = 0.2060; R indices (all data): $R1$ = 0.0896, $wR2$ = 0.2302. **L_2**: $C_{16}H_{24}N_2$, CCDC #736543; M = 244.37, orthorhombic, a = 9.9382(7), b = 35.996(2), c = 8.7463(5) Å, V = 3128.9(4) Å^3, space group *Pbca*, Z = 8, T = 298(2) K, μ (Mo-Kα) = 0.062 mm^{-1}, F(0 0 0) = 1080, GOF = 1.078; final R indices: $R1$ = 0.0724 [$I > 2\sigma(I)$], $wR2$ = 0.1128; R indices (all data): $R1$ = 0.0966, $wR2$ = 0.1616. **L_3**: $C_{18}H_{28}N_2$, CCDC #736544; M = 272.42, orthorhombic, a = 7.700(3), b = 9.950(4), c = 44.635(18) Å, V = 3420(2) Å^3, space group *Pbca*, Z = 8, T = 298(2) K, μ (Mo-Kα) = 0.060 mm^{-1}, F(0 0 0) = 1200, GOF = 0.978; final R indices: $R1$ = 0.0708 [$I > 2\sigma(I)$], $wR2$ = 0.2079; R indices (all data): $R1$ = 0.0939, $wR2$ = 0.2247. **Salt 1**: $C_{14}H_{18}N_2O_4$, CCDC #736545; M = 278.30, monoclinic, a = 17.9579(9), b = 9.5211(5), c = 8.5216(5) Å, V = 1399.51(13) Å^3, space group *Cc*, Z = 4, T = 298(2) K, μ (Mo-Kα) = 0.096 mm^{-1}, F(0 0 0) = 568, GOF = 1.049; final R indices: $R1$ = 0.0553 [$I > 2\sigma(I)$], $wR2$ = 0.1448; R indices (all data): $R1$ = 0.0607, $wR2$ = 0.1505. **Salt 2**: $C_{18}H_{22}N_2O_3S$, CCDC #736546; M = 346.45, orthorhombic, a = 16.2967(8), b = 51.504(3), c = 9.2908(5) Å, V = 7798.2(7) Å^3, space group *Fdd2*, Z = 16, T = 298(2) K, μ (Mo-Kα) = 0.181 mm^{-1}, F(0 0 0) = 2816, GOF = 1.100; final R indices: $R1$ = 0.0547 [$I > 2\sigma(I)$], $wR2$ = 0.1822; R indices (all data): $R1$ = 0.0772, $wR2$ = 0.2104. **Salt 3**: $C_{32}H_{34}N_4O_8$, CCDC #736547; M = 602.63, triclinic, a = 13.5327(4), b = 18.9009(5), c = 20.1113(5) Å, V = 4594.8(2) Å^3, space group *P*-1, Z = 4, T = 298(2) K, μ (Mo-Kα) = 0.063 mm–1, F(0 0 0) = 1892, GOF = 1.022; final R indices: $R1$ = 0.0779 [I _ 2$\sigma(I)$], $wR2$ = 0.1728; R indices (all data): $R1$ = 0.0924, $wR2$ = 0.2146. **Salt 4**: $C_{19}H_{28}N_2O_4$, CCDC #736548; M = 348.43, triclinic, a = 5.3488(4), b = 9.5569(7), c = 19.1994(16) Å, V = 963.43(13) Å^3, space group *P*-1, Z = 2, T = 298(2) K, μ (Mo-Kα) = 0.082 mm^{-1}, F(0 0 0) = 360, GOF = 0.926; final R indices: $R1$ = 0.0607 [$I > 2\sigma(I)$], $wR2$ = 0.1251; R indices (all data): $R1$ = 0.0942, $wR2$ = 0.1971. **Salt 5**: $C_{84}H_{105}N_8O_{16}$, CCDC #736549; M = 1482.76, triclinic, a = 12.8838(4), b = 16.4270(5), c = 19.2316(5) Å, V = 4024.0(2) Å^3, space group *P*-1, Z = 2, T = 298(2) K, μ (Mo-Kα) = 0.088 mm^{-1}, F(0 0 0) = 1736, GOF = 1.037; final R indices: $R1$ = 0.0688 [$I > 2\sigma(I)$], $wR2$ = 0.2036; R indices (all data): $R1$ = 0.0801, $wR2$ = 0.2440. **Salt 6**: $C_{50}H_{72}N_4O_7S_2$, CCDC #736550; M = 905.26, monoclinic, a = 16.2311(11), b = 9.0989(7), c = 36.055(3) Å, V = 5308.4(7) Å^3, space group *C2/c*, Z = 4, T = 298(2) K, μ (Mo-Kα) = 0.148 mm^{-1}, F(0 0 0) = 1912, GOF = 1.0649; final R indices: $R1$ = 0.0659 [$I > 2\sigma(I)$], $wR2$ = 0.2168; R indices (all data): $R1$ = 0.0822, $wR2$ = 0.2332. The crystallographic data for the complexes have been deposited with the Cambridge Crystallographic Data Centre. Copies of this information may be obtained free of charge from the Director, CCDC, 12 Union Road, Cambridge, CB2 1EZ, UK (fax: +44 1223 336033, e-mail: deposit@ccdc.cam.ac.uk or http://www.ccdc.cam.ac.uk).